ACS OMEGA

Article

Cite This: ACS Omega 2018, 3, 5229−5236

# Single Crystal Growth of Hybrid Lead Bromide Perovskites Using a Spin-Coating Method

Rocío García-Aboal, Roberto Fenollosa, Fernando Ramiro-Manzano, Isabelle Rodríguez, Francisco Meseguer, and Pedro Atienzar*

Instituto Universitario de Tecnologia Química, CSIC-UPV, Universitat Politècnica de València, Av. de los Naranjos, Valencia 46022, Spain

Supporting Information

**ABSTRACT:** Synthesis and studies of single crystals of hybrid perovskite are important for achieving a better understanding of the optoelectronic phenomena occurring in this material and for improving ongoing applications. Here, we report on the growth of micrometer-size single crystals of methylammonium lead bromide ($MAPbBr_3$) using the spin coating deposition method on a quartz substrate. We studied the influence of the rotation speed and the use of three different additives *N*-cyclohexyl-2-pyrrolidone, dimethyl sulfoxide, and 4-*tert*-butylpyridine on the crystal size and shape. The introduction of an additive in the precursor solution is revealed to be very useful for obtaining crystals with well-defined geometries and for decreasing the amount of defects. In this way, high-quality single crystals that sustain optical resonating modes were obtained and characterized by transmittance and photoluminescence measurements.

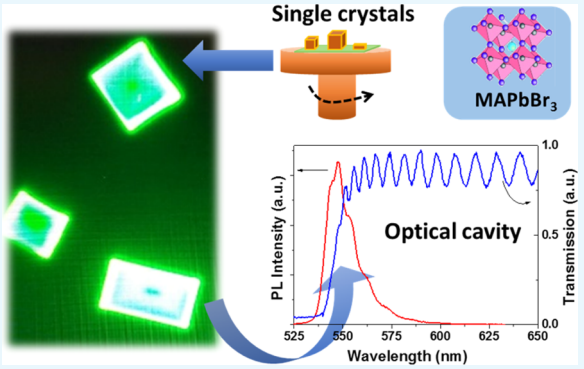


## 1. INTRODUCTION

In the last years, hybrid perovskites[1,2] have attracted a great interest because of their potential application in the field of photovoltaics, where, in a reduced period of time, they reached efficiencies over 22%,[3] a value that exceeds other emerging technologies, such as quantum dots, dye-sensitized solar cells, or organic solar cells.[4,5] These materials have some advantages, such as ease of processing and low fabrication cost. Their synthesis can be attained through various routes like those based on solution[1] and vapor-assisted[6] methods. However, they also have some limitations, such as poor stability or toxicity of the components. In this context, delicate control over the crystal formation has been shown to play a key role in the physical properties and therefore in the reproducibility and efficiency[2] of perovskite-based solar cells. Here, we study the formation and the properties of hybrid lead bromide perovskite single crystals. There are several methods for the synthesis of single crystals, such as inverse temperature crystallization,[7] antisolvent-assisted crystallization techniques,[8] and top-seeded solution growth method[9,10] among others. In this work, we used the spin coating method[11−13] because it is fast, versatile, reproducible, inexpensive, and finally it requires moderate amounts of reactant. Although the size of the obtained crystals is in the micrometer range, they are large enough to study their physical and chemical properties and could be used to develop photovoltaic devices with appropriate grain size. In contrast, most of the studies in this respect have been done in large single crystals with millimeter size, which require long preparation time and several processing steps.[8,14]

Although there are many parameters of the spin coating method influencing the formation of perovskites, such as rotation speed, annealing, concentration of precursors, solvents, and atmosphere,[15] among others, here we focus on the influence of the speed of rotation and the admixture of three different additives to the basic precursor compounds. Recent studies have shown that the use of highly miscible low-vapor-pressure additives is very effective for improving perovskite crystallization[2,15,16] because they decrease the rate of evaporation of the precursor solution solvent. On the basis of previous results concerning the preparation of active layers of perovskite in photovoltaic devices, we selected dimethylformamide (DMF) as the main solvent and three different additives for the synthesis of single crystals. In general, all of the additives have in common both the ability to be coordinated with the precursors and a high boiling point. The first additive is *N*-cyclohexyl-2-pyrrolidone (CHP),[2] which at low concentration induces homogeneous crystal nucleation and growth, favoring high reproducibility. It has a particularly high boiling point (284 °C) and low vapor pressure. The second investigated additive is 4-*tert*-butylpyridine (TBP). Shi et al. added this compound in the precursor solution, resulting in a better crystallinity and a

Received: March 9, 2018
Accepted: April 19, 2018
Published: May 15, 2018






DOI: 10.1021/acsomega.8b00447
ACS Omega 2018, 3, 5229−5236

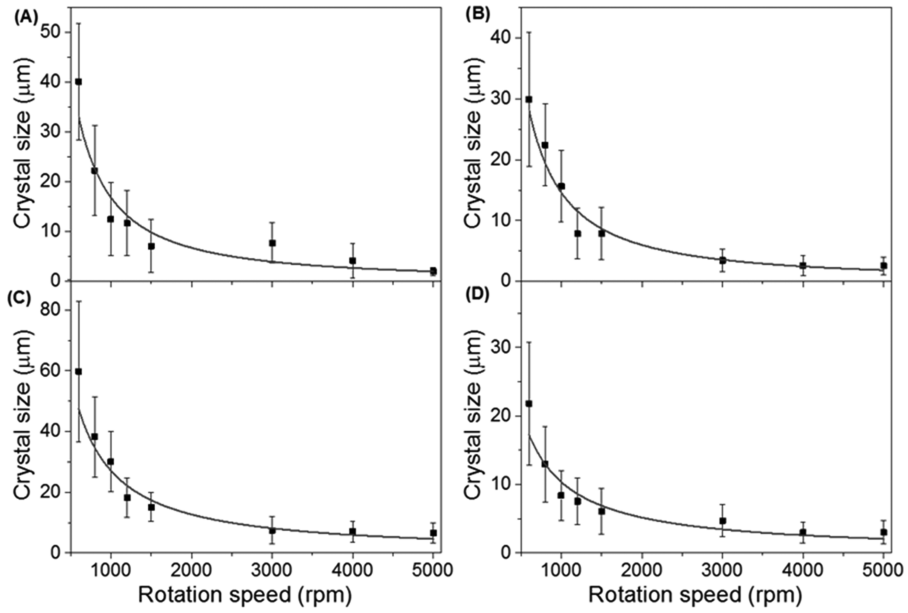


**Figure 1.** Average crystal size (dots) as a function of the spin coater rotation speed for a precursor solution without additive (A) and with (B) CHP, (C) DMSO, and (D) TBP as additive. The error bars correspond to the standard deviation provided by statistical methods. The gray lines correspond to fits of experimental data to functions like ($\propto 1/\text{speed}^{\gamma}$), and the fitted values of $\gamma$ are 1.3, 1.2, 1.2, and 0.9 for (A)−(D), respectively.

**Table 1. Properties of the Solvent and Additives Used in the Present Study**

| Compound | Structure | Boiling Point (°C) | Vapor pressure (mmHg, 25°C) | Viscosity (cPoise) |
|---|---|---|---|---|
| Dimethylformamide (DMF) | 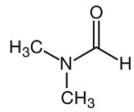 | 155 | 2.9 | 0.92 |
| N-cyclohexyl-2-pyrrolidone (CHP) | 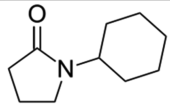 | 284-304 | 0.05 | 11.6 |
| Dimethyl Sulfoxide (DMSO) | 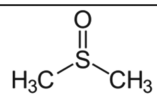 | 189 | 0.42 | 0.7 |
| 4-tert-Butylpyridine (TBP) | 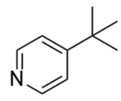 | 197 | 4.53 | 1.5 |

more homogeneous orientation of the crystals. This is probably due to the coordination of such compound with the $Pb^{2+}$ atoms and its role as dispersing agent, which avoids the formation of aggregates.[16] Finally, we consider dimethyl sulfoxide (DMSO) as an interesting additive because it can coordinate easily to the $PbBr_2$ precursor.[17]

Optical properties are closely related to the performance of photovoltaic devices. Therefore, we have undertaken as a characterization strategy of the crystals the study of their optical properties, particularly photoluminescence and transmittance, at the single-crystal level, using for that purpose a homemade setup[7] that allows us to test their behavior as optical cavities.

## 2. RESULTS AND DISCUSSION

**2.1. Influence of Rotation Speed and Additive.** The synthesis procedure based on the spin coating process, under the specified conditions detailed in Section 4, produces well-isolated single crystals. Figure 1 shows the variation of the average size of the obtained crystals (black dots) with the speed



DOI: 10.1021/acsomega.8b00447
ACS Omega 2018, 3, 5229−5236

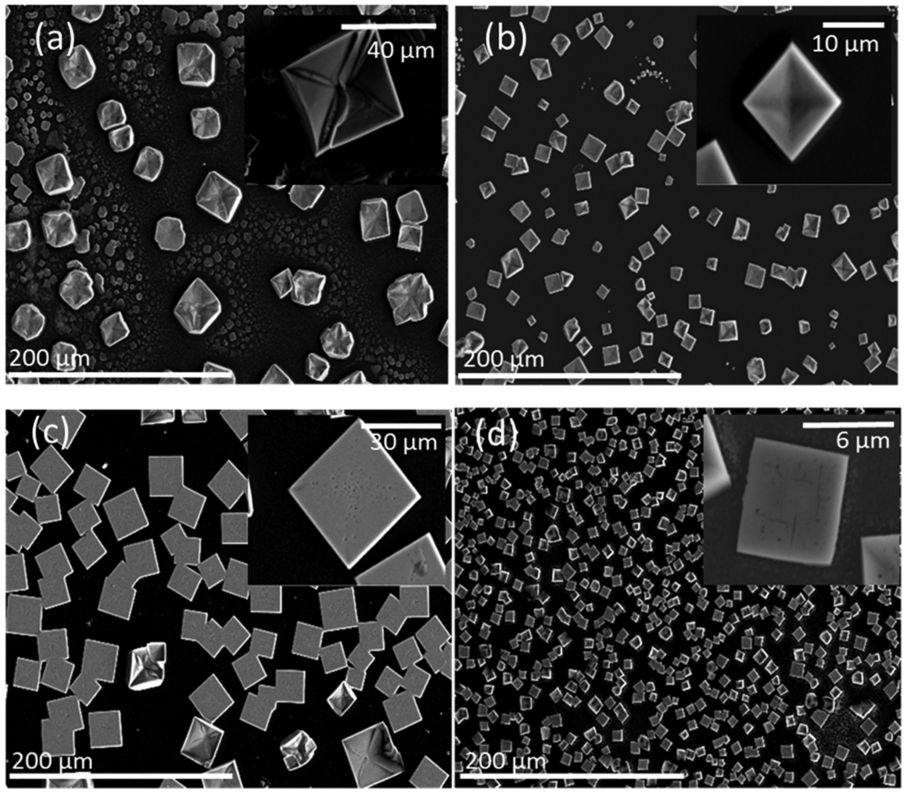


**Figure 2.** Scanning electron microscopy (SEM) images of $MAPbBr_3$ crystals grown on quartz substrates by spin coating at 1000 rpm, corresponding to samples NA (a), CHP (b), DMSO (c), and TBP (d).

of the spin coater under different conditions: (a) without additive (NA) and with different additives (b) CHP, (c) DMSO, and (d) TPB. The error bars correspond to the standard deviation of each value obtained by statistical means (see Section 4). The as-synthesized crystals are polydisperse in size, in some cases with a dispersion value of about 50%, regardless of the rotation speed and precursor solution. However, in general, the average size of the crystals decreases as the rotation speed increases, following a law (gray curves) like ($\propto 1/\text{speed}^{\gamma}$) with different values of the exponent $\gamma$, which are indicated in the caption of Figure 1. Such law is typical for the thickness of a deposited layer by spin coating, but with $\gamma = 1/2$. We think that the distinct values of $\gamma$ obtained for the crystal size stem from the fact that the growth of the crystals includes different stages, where the removal of the excess of solvent as a consequence of the centrifugal force is followed by an evaporation process that increases the viscosity and the precursors concentration. Nevertheless, the experiments indicate that the quicker the solvent evaporation, the larger the number of crystal nucleation points, which results in a reduced average crystal size.

We did not find any clear relation between the size of the crystals and the physical properties of the additives (Table 1, Section 4). Nevertheless, those solutions containing DMSO as additive produced the largest crystals, specially at low rotation speeds, whereas solutions with TBP as additive yielded the smallest ones. It can be explained by considering the different ability of coordination with $Pb^{2+}$ and the solubility of the precursors. Shi et al.[16] indicated that the nitrogen atom on TBP favors the coordination with $Pb^{2+}$ with respect to the oxygen atom on DMF, thus hindering the formation of large bulks and aggregates and favoring, therefore, the formation of small crystals. All of the above is relevant to the preparation of highly efficient photovoltaic solar cells, considering that there is an optimum crystal size depending on the device configuration, and in general, large crystals are desired due to lower $J-V$ hysteresis and less charge trapping and recombination at the grain boundaries.[18,19]

Figure 2a–d shows scanning electron microscopy (SEM) images of methylammonium lead bromide ($MAPbBr_3$) crystals grown on quartz substrates by spin coating at 1000 rpm, corresponding to samples NA, CHP, DMSO, and TBP respectively. All of the samples contain well-isolated single crystals that are pyramid-shaped in general. However, crystals having other shapes, namely, rods and plates, grow as well, at the same time. Plate-shaped structures are particularly interesting for testing the properties of the crystals as photonic microcavities, as we will see below. We found that, in general, the use of an additive in the precursor solution produces crystals with better-defined geometries and with less defects (Figure 2b–d) compared to those obtained without any additive (Figure 2a). This effect is even more pronounced for the CHP additive, and it should be taken into account for the study of the optical properties, which can be strongly influenced by the geometry and structural defects of the crystals.

X-ray diffraction (XRD) measurements (Figure 3) show that all of the synthesized samples have in fact a crystalline nature with a characteristic cubic structure finger print ($Pm\bar{3}m$).[20] In contrast to samples NA and TPB, samples DMSO and CHP show the appearance of (110) and (210) peaks, suggesting that the crystals are highly oriented[8,21] with the planes parallel to the substrate. This feature occurs for all of the rotation speeds. It is very interesting because it is well demonstrated that more oriented domains of perovskites in photovoltaic devices



DOI: 10.1021/acsomega.8b00447
ACS Omega 2018, 3, 5229–5236

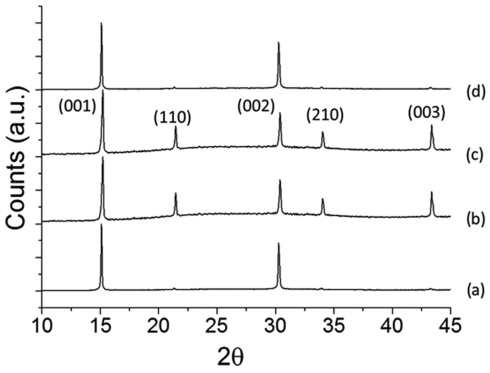


**Figure 3.** XRD pattern of a layer of crystals of (a) NA, (b) CHP, (c) DMSO, and (d)TBP samples.

increase their photocurrent and therefore their final performance.[22]

The photoluminescence properties of the synthesized crystals were found to be influenced by the type of additive used in the precursor solution rather than by the rotation speed. Figure 4a–d shows optical microscopy images at 40× magnification of samples NA, CHP, DMSO, and TBP, respectively, for a rotation speed of 1000 rpm, and Figure 4e–h shows their corresponding photoluminescence images. Optical microscopy images of all of the samples for all of the studied rotation speeds can be seen in the Supporting Information (Figures S1–S4).

Samples CHP and TBP yield a bright green photoluminescence signal, whereas samples NA and DMSO give, in general, less intense signals. We attributed this effect to the amount of surface states produced during the crystallization process, which act as nonradiative recombination centers. This is an important result to be considered in future developments because such centers are strongly influenced by environmental conditions of moisture and light.[23] Figure 5A shows the optical absorbance and Figure 5B shows the normalized photoluminescence spectra of the sample areas of Figure 4. They are similar to those of previous reports of hybrid lead bromide perovskites,[24−26] but slight differences in the position of the peak maximum and the asymmetry have arisen. Although samples NA and TBP yielded a quite symmetric peak, with the maximum position at 535 nm, the peak maxima for samples CHP and DMSO were red-shifted to 540 nm and they showed some asymmetric features, which consist of shoulders placed at about 552 nm and in the range of ca. 555−600 nm. Although a complete elucidation of these effects has not been achieved yet, we think they are related to the aging of the surface or structural inhomogeneities in the crystals[24,26,27] and to light reabsorption mechanisms.[28,29]

**2.2. Synthesis of Rod-Shaped Crystals.** Rod-shaped single crystals were found in small amounts in sample CHP, especially at low rotation speeds. We studied the influence of the concentration of this particular additive in the precursor solution on the crystal formation. Figure 6 shows representative optical microscopy images of the obtained crystals for different CHP concentrations, from 5 to 60% v/v in DMF. Moreover, Figure 7B shows the variation of the average size of the crystals and the ratio of rod/cuboid-shaped crystals with respect to the CHP concentration. At low concentrations, square-like plates are dominant. However, for increasing values of the CHP content, the formation of wirelike structures is favored and the size of the plates is reduced. This was attributed to the fact that CHP contains a significant apolar region because of the cyclohexyl ring, thus inducing a preferential direction of growth probably due to screw dislocation defects.[30] A similar trend has been discussed for the preparation of other 1D structures.[31,32] On the other hand, no significant variation in crystal growth has been observed in the case of DMSO and TBP additives when their concentration was increased.

The influence of the rotation speed on the formation of rod-shaped crystals was studied for the 5% CHP vol/vol concentration in DMF precursor solution. As mentioned above, the growth of rod-shaped crystals is, in general, favored by low rotation speeds. This indicates that low evaporation rates of the solvent are required for them to be able to grow. Such a formation process has been observed by using low evaporation rates in the drop casting method (see video in the Supporting Information). Moreover, we have found a threshold rotation speed, at about 1000 rpm, which defines two main regions where crystals grow differently (Figure 7A,B). Most of the crystals, say 80%, grow either in rod- or cuboid-like shapes depending on the rotation speed region, low or high, respectively, where they were synthesized. An explanation of this threshold value constitutes currently an object of research.

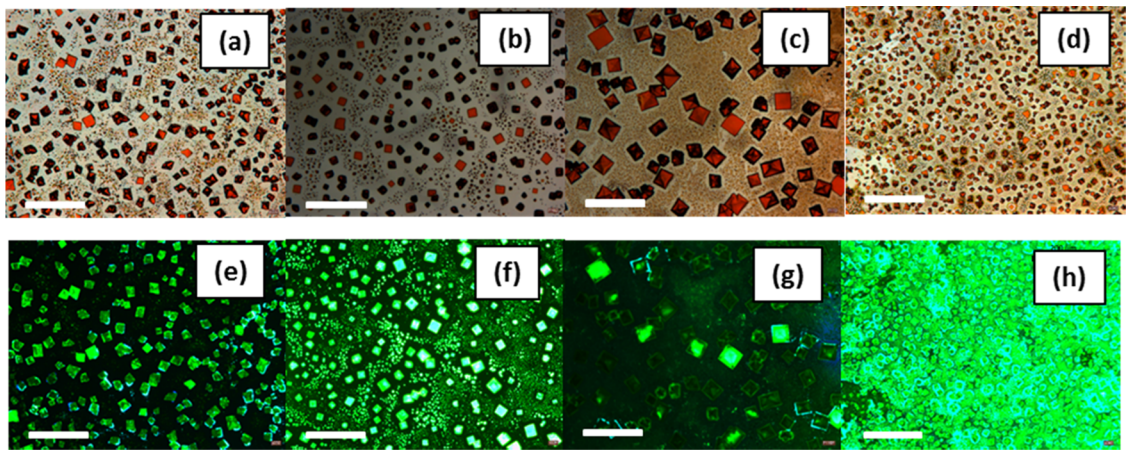


**Figure 4.** (a)–(d) Optical microscopy images at 40× magnification of samples NA, CHP, DMSO, and TBP, respectively, for a rotation speed of 1000 rpm. (e–h) The corresponding photoluminescence images. The scale bars correspond to 200 μm.



DOI: 10.1021/acsomega.8b00447
ACS Omega 2018, 3, 5229−5236

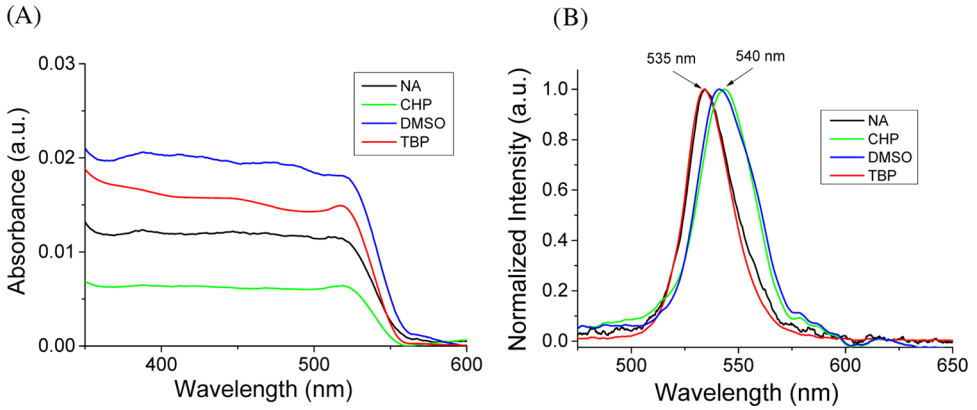


**Figure 5.** (A) UV–vis absorption spectra and (B) photoluminescence spectra of the sample areas of Figure 4, corresponding to samples NA, CHP, DMSO, and TBP.

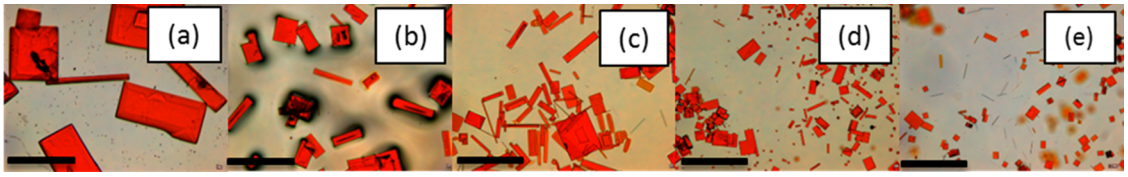


**Figure 6.** Optical microscopy images of crystals synthesized by increasing concentrations of CHP additive: (a) 5, (b) 15, (c) 25, (d) 50, and (e) 60% v/v in DMF. The scale bars correspond to 200 $\mu$m.

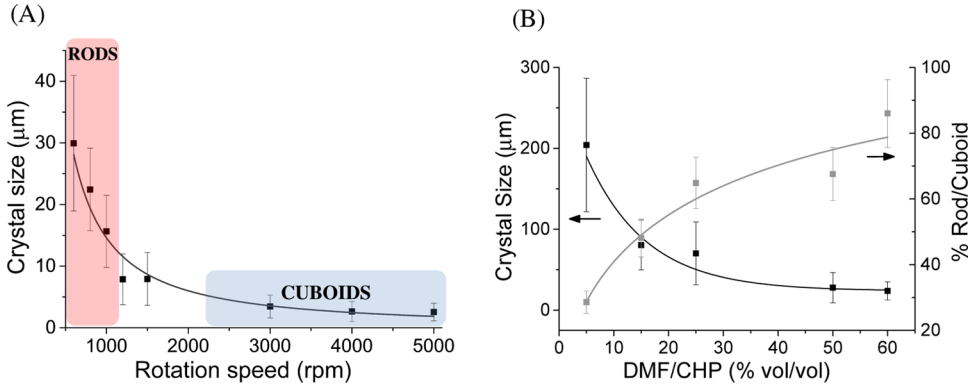


**Figure 7.** (A) Curve of average crystal size vs spin coater rotation speed obtained by using 5% of CHP additive vol/vol concentration in DMF for the precursor solution. The two shaded areas indicate two regimes where crystals grow differently: in rod- or cuboid-like shapes. (B) Curves of average crystal size (black line) and rod/cuboids ratio (gray line) as a function of the CHP additive concentration. The error bars correspond to the standard deviation provided by statistical methods.

**2.3. Optical Properties of Single Crystals.** A good proof for testing the quality of a crystal is its ability to sustain optical resonant modes because such modes can be strongly influenced by crystal defects. In general, the better the quality of a crystal, the more pronounced are its optical resonances. However, they also depend on other factors like the coupling of light, the absorption of the material itself, and more importantly the geometry of the crystal, particularly the size of the crystal compared to the wavelength of light, and how its faces are orientated each other. Resonant conditions should allow a kind of feedback cycle of light inside the crystal, which is produced by multiple reflections at the crystal faces and finally leads to an interference phenomenon. In this way, a pyramid-shaped crystal is not expected to sustain any resonance because of its intricate geometry. However, the parallel faces of a plate-shaped crystal are optimum for producing Fabry–Perot-type resonances.[27] Figure 8a shows the photoluminescence (black curve) and the optical transmittance (red curve) spectra of a plate-shaped crystal, which was synthesized at 800 rpm by using CHP as additive. Figure 8b shows an image of the measured crystal obtained by optical microscopy. It has well-defined parallel faces with dimensions of 20.64 × 21.62 $\mu$m$^2$ in area and 1.5 $\mu$m in depth, as deduced from a modeling process.[33] As expected, interference ripples appear in the transmittance spectrum in that range from where the absorption of the material somehow diminishes, say about 550 nm to longer wavelengths, thus confirming that the crystal itself can work as an optical microcavity, and it has a good structural quality. The photoluminescence spectrum shows ripples as well, coinciding with those of the transmittance spectrum, but they are less pronounced because of differences between the envelope curves.[33] Figure 8c shows for comparison the transmittance and photoluminescence spectra of a pyramid-shaped crystal (Figure 8d), where no resonances could be detected. In any case, it is interesting for future developments to take into account these



DOI: 10.1021/acsomega.8b00447
ACS Omega 2018, 3, 5229–5236

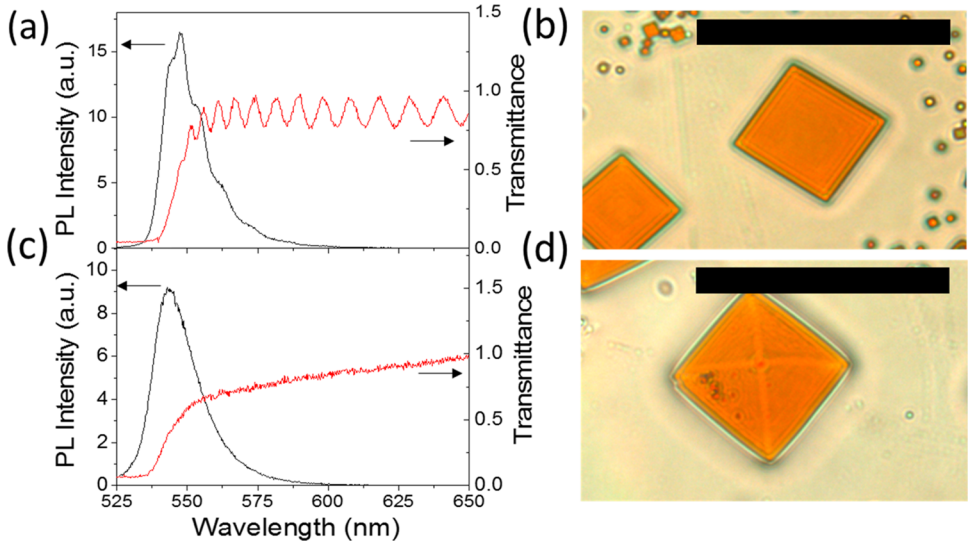


**Figure 8.** Photoluminescence (black curve) and transmittance (red curve) spectra of (a) plate-shaped crystal and (c) pyramid-shaped crystal. (b, d) The corresponding optical microscopy images. The scale bars correspond to 50 $\mu$m.

resonant effects at the single-crystal level, which in our opinion could help increase the efficiency of perovskite-based solar cells.

## 3. CONCLUSIONS

We have described the synthesis and characterization of single crystals of $MAPbBr_3$ prepared by a spin coating method at different rotation speeds. In addition, we studied the influence of three different additives previously used in high-performance inorganic−organic hybrid perovskite solar cells. We observed that the use of additives, particularly CHP, produces crystals with a better-defined geometry and with less defects, compared to crystals obtained without any additive, and at the same time, CHP and DMSO additives have a tendency to produce more oriented crystals. Also, we showed that increasing the concentration of CHP additive results in the formation of rods of $MAPbBr_3$. Finally, we demonstrated that single crystals of $MAPbBr_3$ prepared by this methodology can behave as resonating cavities.

## 4. EXPERIMENTAL SECTION

**4.1. Materials.** The precursors lead bromide ($PbBr_2$) and methylammonium bromide (MABr); the main solvent dimethylformamide (DMF); and the three additives *N*-cyclohexyl-2-pyrrolidone (CHP), 4-*tert*-butylpyridine (TBP), and dimethyl sulfoxide (DMSO) are obtained from Sigma-Aldrich. They were used as received. Table 1 summarizes the physical properties of the solvent and additives.

**4.2. Synthesis of $MAPbBr_3$ Perovskite Single Crystals.** Precursor solutions were prepared by dissolving stoichiometric mixtures of 1 M MABr and 1 M $PbBr_2$ in DMF,[34] namely, 120 mg of MABr and 370 mg of $PbBr_2$ in 2 mL of DMF. In the case of solutions containing an additive (CHP, TBP, or DMSO), 20 $\mu$L thereof was added into 380 $\mu$L of the precursor solution, resulting in a concentration of about 5 vol %. In addition, for CHP, the concentration was increased to obtain solutions with 15, 25, 50, and 60 vol %.

$MAPbBr_3$ crystals were grown by a spin coating process on quartz substrates of area $\approx$ 1 $cm^2$. To increase the hydrophilicity of the surface, the substrates had been previously treated with hydrochloridric acid and cleaned with acetone and isopropanol, followed by exhaustive rinsing with distilled water. The spin coating process was performed at room temperature and in a controlled nonoxidizing atmosphere at different spin speed rates, in the range of 600−5000 rpm. In all of the synthesis experiments, a volume of 20 $\mu$L of precursor solution was dropped in the middle of the substrate before the rotation process had started. Then, the spinner was turned on, producing a homogeneous distribution of the precursor solution through the substrate, thus favoring the efficient removal of the solvent and giving rise to the formation of crystals. We kept the rotation process on for 2 min, and after that, the substrates containing the as-grown crystals were annealed for further 2 min at 90 °C so as to remove completely any rest of solvent.

**4.3. Optical Microscopy and Photoluminescence of Polycrystalline Samples.** General views of the as-grown crystals were obtained at different magnifications by an optical microscope (Leica DM4000). It includes a module for fluorescence characterization, which consists of a mercury lamp and a Leica bandpass filter (340−380 nm) as illumination source, and an Avantes AvaSpec-2048 Fiber Optic Spectrometer, which provides a resolution better than 0.5 nm. Photoluminescence of sample areas containing many crystals were obtained by using this setup.

**4.4. X-ray Diffraction Experiments.** X-ray polycrystalline film diffraction patterns of the samples were collected by a Bruker D8 Advance A25 X-ray diffractometer operating at 45 kV and 80 mA Cu K$\alpha$ radiation ($\lambda$ = 1.5406 Å) equipped with a LYNXEYE XE 1-D detector. It records the diffraction signal of an area of 3 mm × 3 mm. No signals from the quartz substrate were detected.

**4.5. Optical Characterization of Single Crystals.** The optical properties, specifically photoluminescence and transmittance, of single crystals were obtained by means of a homemade setup (see Figure 9). Basically, it includes two branches, one for excitation and the other one for collection purposes, both focused by 20× Mitutoyo objectives at the same spot, with a typical size of about 1 $\mu$m. In the experiments reported here, both branches were oriented so that the collected light was in forward direction with respect to the incident or exciting light. The collection branch includes an iris,



DOI: 10.1021/acsomega.8b00447
*ACS Omega* 2018, 3, 5229−5236

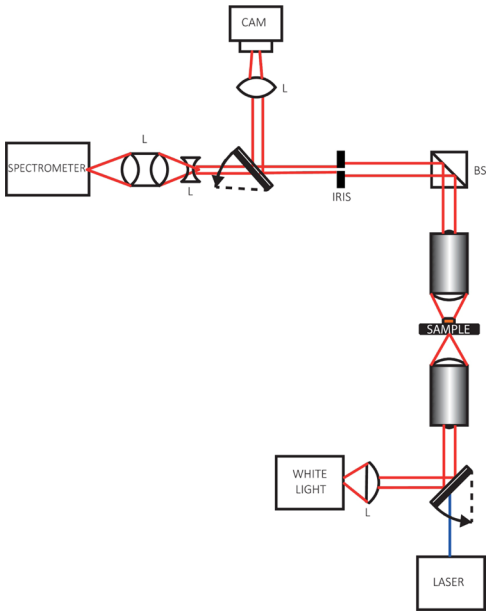


**Figure 9.** Schematic representation of the setup used for measuring the OT and PL spectra, where the different acronyms are lens (L), beam splitter (BS), spectrometer, and camera (CAM).

where the spot is focused. It allows selecting the signal from a sample area of micrometer range and even submicrometer range. After the iris, a motorized mirror drives the signal either to a charge-coupled device (CCD) camera, by means of which, the exact part of crystal being examined can be visualized, or to a spectrometer (iHR320-HORIBA), which is equipped with a liquid nitrogen refrigerated Si-CCD, and it is used for measuring the spectrum of the collected light.

White light of a halogen lamp was used for transmittance experiments, whereas excitation light of 405 nm wavelength, provided by a solid-state laser, was used for photoluminescence experiments. In all of the cases, we worked with a moderate intensity of about 0.1 mW for avoiding fast crystal degradation.

Two types of crystal geometries were measured: pyramid- and plate-shaped samples. In both cases, the crystal was oriented so that the largest face of the crystal was perpendicular to the incident or collected light.

**4.6. Crystal Size Measurement Procedure.** An optical microscope (Leica DM4000) was used to obtain a general overview of the crystal size and shape. Three samples were synthesized and studied for each speed/additive condition. Once the uniformity of each sample had been guaranteed by analyzing different sample areas, 60−80 crystals therein were measured by using the ImageJ software. We considered for each single crystal the sample area, which is parallel to the substrate, and measured the length of one of its sides. In those cases, where the area had a rectangular shape, like, for instance, in rods, we measured the longer dimension. Histograms for each synthesis condition were obtained by considering all of the measurements of the three corresponding samples, which showed good reproducibility without significant differences in any case. The crystal size parameter was divided into five ranges in the histograms, and the obtained mode and standard deviation values are plotted in Figure 1. Also, they are detailed in Table S1 of the Supporting Information.

## ■ ASSOCIATED CONTENT

### Supporting Information

The Supporting Information is available free of charge on the ACS Publications website at DOI: 10.1021/acsomega.8b00447.

Optical microscopy images (Figures S1−S4) and size and standard deviation of samples (Table S1) (PDF)

Crystal formation (MPG)

## ■ AUTHOR INFORMATION

### Corresponding Author

*E-mail: patienzar@itq.upv.es.

### ORCID

Pedro Atienzar: 0000-0002-0356-021X

### Notes

The authors declare no competing financial interest.

## ■ ACKNOWLEDGMENTS

Financial support from the Spanish Ministry of Economy and Competitiveness (Severo Ochoa, SEV-2016-0683), Intramural CSIC project 201680I006, and Fundación Ramón Areces (XVII Concurso Nacional para la adjudicación de Ayudas a la Investigación en Ciencias de la Vida y de la Materia) is gratefully acknowledged. Financial support was also provided by the Spanish Ministry of Economy and Competitiveness (Mineco) of Spain (TEC2015-74405-JIN), MAT2015-69669-P, and regional government grant PrometeoII/2017/026.

## ■ REFERENCES

(1) Lee, M. M.; Teuscher, J.; Miyasaka, T.; Murakami, T. N.; Snaith, H. J. Efficient Hybrid Solar Cells Based on Meso-Superstructured Organometal Halide Perovskites. *Science* **2012**, *338*, 643−647.

(2) Jeon, Y.-J.; Lee, S.; Kang, R.; Kim, J.-E.; Yeo, J.-S.; Lee, S.-H.; Kim, S.-S.; Yun, J.-M.; Kim, D.-Y. Planar heterojunction perovskite solar cells with superior reproducibility. *Sci. Rep.* **2014**, *4*, No. 6953.

(3) Yang, W. S.; Park, B.-W.; Jung, E. H.; Jeon, N. J.; Kim, Y. C.; Lee, D. U.; Shin, S. S.; Seo, J.; Kim, E. K.; Noh, J. H.; Seok, S. I. Iodide management in formamidinium-lead-halide−based perovskite layers for efficient solar cells. *Science* **2017**, *356*, 1376−1379.

(4) Albero, J.; Atienzar, P.; Corma, A.; Garcia, H. Efficiency Records in Mesoscopic Dye-Sensitized Solar Cells. *Chem. Rec.* **2015**, *15*, 803−828.

(5) Lu, L.; Zheng, T.; Wu, Q.; Schneider, A. M.; Zhao, D.; Yu, L. Recent Advances in Bulk Heterojunction Polymer Solar Cells. *Chem. Rev.* **2015**, *115*, 12666−12731.

(6) Ávila, J.; Momblona, C.; Boix, P. P.; Sessolo, M.; Bolink, H. J. Vapor-Deposited Perovskites: The Route to High-Performance Solar Cell Production? *Joule* **2017**, *1*, 431−442.

(7) Saidaminov, M. I.; Abdelhady, A. L.; Murali, B.; Alarousu, E.; Burlakov, V. M.; Peng, W.; Dursun, I.; Wang, L.; He, Y.; Maculan, G.; Goriely, A.; Wu, T.; Mohammed, O. F.; Bakr, O. M. High-quality bulk hybrid perovskite single crystals within minutes by inverse temperature crystallization. *Nat. Commun.* **2015**, *6*, No. 7586.

(8) Shi, D.; Adinolfi, V.; Comin, R.; Yuan, M.; Alarousu, E.; Buin, A.; Chen, Y.; Hoogland, S.; Rothenberger, A.; Katsiev, K.; Losovyj, Y.; Zhang, X.; Dowben, P. A.; Mohammed, O. F.; Sargent, E. H.; Bakr, O. M. Low trap-state density and long carrier diffusion in organolead trihalide perovskite single crystals. *Science* **2015**, *347*, 519−522.

(9) Dong, Q.; Fang, Y.; Shao, Y.; Mulligan, P.; Qiu, J.; Cao, L.; Huang, J. Electron-hole diffusion lengths >175 $\mu$m in solution-grown $CH_3NH_3PbI_3$ single crystals. *Science* **2015**, *347*, 967−970.

(10) Dang, Y.; Zhou, Y.; Liu, X.; Ju, D.; Xia, S.; Xia, H.; Tao, X. Formation of Hybrid Perovskite Tin Iodide Single Crystals by Top-Seeded Solution Growth. *Angew. Chem., Int. Ed.* **2016**, *55*, 3447−3450.

(11) Emslie, A. G.; Bonner, F. T.; Peck, L. G. Flow of a Viscous Liquid on a Rotating Disk. *J. Appl. Phys.* **1958**, *29*, 858−862.



DOI: 10.1021/acsomega.8b00447
*ACS Omega* 2018, 3, 5229−5236

(12) Meyerhofer, D. Characteristics of resist films produced by spinning. *J. Appl. Phys.* **1978**, *49*, 3993−3997.
(13) Lawrence, C. J. The mechanics of spin coating of polymer-films. *Phys. Fluids* **1988**, *31*, 2786−2795.
(14) Dang, Y.; Liu, Y.; Sun, Y.; Yuan, D.; Liu, X.; Lu, W.; Liu, G.; Xia, H.; Tao, X. Bulk crystal growth of hybrid perovskite material CH3NH3PbI3. *CrystEngComm* **2015**, *17*, 665−670.
(15) Cohen, B.-E.; Etgar, L. Parameters that control and influence the organo-metal halide perovskite crystallization and morphology. *Front. Optoelectron.* **2016**, *9*, 44−52.
(16) Shi, Y.; Wang, X.; Zhang, H.; Li, B.; Lu, H.; Ma, T.; Hao, C. Effects of 4-tert-butylpyridine on perovskite formation and performance of solution-processed perovskite solar cells. *J. Mater. Chem. A* **2015**, *3*, 22191−22198.
(17) Li, W.; Fan, J.; Li, J.; Mai, Y.; Wang, L. Controllable Grain Morphology of Perovskite Absorber Film by Molecular Self-Assembly toward Efficient Solar Cell Exceeding 17%. *J. Am. Chem. Soc.* **2015**, *137*, 10399−10405.
(18) Kim, H.-S.; Park, N.-G. Parameters Affecting I−V Hysteresis of CH3NH3PbI3 Perovskite Solar Cells: Effects of Perovskite Crystal Size and Mesoporous TiO2 Layer. *J. Phys. Chem. Lett.* **2014**, *5*, 2927−2934.
(19) Salim, T.; Sun, S.; Abe, Y.; Krishna, A.; Grimsdale, A. C.; Lam, Y. M. Perovskite-based solar cells: impact of morphology and device architecture on device performance. *J. Mater. Chem. A* **2015**, *3*, 8943−8969.
(20) Zhu, Q.; Zheng, K.; Abdellah, M.; Generalov, A.; Haase, D.; Carlson, S.; Niu, Y.; Heimdal, J.; Engdahl, A.; Messing, M. E.; Pullerits, T.; Canton, S. E. Correlating structure and electronic band-edge properties in organolead halide perovskites nanoparticles. *Phys. Chem. Chem. Phys.* **2016**, *18*, 14933−14940.
(21) Cho, N.; Li, F.; Turedi, B.; Sinatra, L.; Sarmah, S. P.; Parida, M. R.; Saidaminov, M. I.; Murali, B.; Burlakov, V. M.; Goriely, A.; Mohammed, O. F.; Wu, T.; Bakr, O. M. Pure crystal orientation and anisotropic charge transport in large-area hybrid perovskite films. *Nat. Commun.* **2016**, *7*, No. 13407.
(22) Docampo, P.; Hanusch, F. C.; Giesbrecht, N.; Angloher, P.; Ivanova, A.; Bein, T. Influence of the orientation of methylammonium lead iodide perovskite crystals on solar cell performance. *APL Mater.* **2014**, *2*, No. 081508.
(23) Brenes, R.; Guo, D.; Osherov, A.; Noel, N. K.; Eames, C.; Hutter, E. M.; Pathak, S. K.; Niroui, F.; Friend, R. H.; Islam, M. S.; Snaith, H. J.; Bulović, V.; Savenije, T. J.; Stranks, S. D. Metal Halide Perovskite Polycrystalline Films Exhibiting Properties of Single Crystals. *Joule* **2017**, *1*, 155−167.
(24) Chen, F.; Zhu, C.; Xu, C.; Fan, P.; Qin, F.; Gowri Manohari, A.; Lu, J.; Shi, Z.; Xu, Q.; Pan, A. Crystal structure and electron transition underlying photoluminescence of methylammonium lead bromide perovskites. *J. Mater. Chem. C* **2017**, *5*, 7739−7745.
(25) Saidaminov, M. I.; Adinolfi, V.; Comin, R.; Abdelhady, A. L.; Peng, W.; Dursun, I.; Yuan, M.; Hoogland, S.; Sargent, E. H.; Bakr, O. M. Planar-integrated single-crystalline perovskite photodetectors. *Nat. Commun.* **2015**, *6*, No. 8724.
(26) Wang, K.-H.; Li, L.-C.; Shellaiah, M.; Wen Sun, K. Structural and Photophysical Properties of Methylammonium Lead Tribromide (MAPbBr3) Single Crystals. *Sci. Rep.* **2017**, *7*, No. 13643.
(27) Grancini, G.; D'Innocenzo, V.; Dohner, E. R.; Martino, N.; Srimath Kandada, A. R.; Mosconi, E.; De Angelis, F.; Karunadasa, H. I.; Hoke, E. T.; Petrozza, A. CH3NH3PbI3 perovskite single crystals: surface photophysics and their interaction with the environment. *Chem. Sci.* **2015**, *6*, 7305−7310.
(28) Diab, H.; Arnold, C.; Lédée, F.; Trippé-Allard, G.; Delport, G.; Vilar, C.; Bretenaker, F.; Barjon, J.; Lauret, J.-S.; Deleporte, E.; Garrot, D. Impact of Reabsorption on the Emission Spectra and Recombination Dynamics of Hybrid Perovskite Single Crystals. *J. Phys. Chem. Lett* **2017**, *8*, 2977−2983.
(29) Fang, Y.; Wei, H.; Dong, Q.; Huang, J. Quantification of re-absorption and re-emission processes to determine photon recycling efficiency in perovskite single crystals. *Nat. Commun.* **2017**, *8*, No. 14417.
(30) Meng, F.; Morin, S. A.; Forticaux, A.; Jin, S. Screw Dislocation Driven Growth of Nanomaterials. *Acc. Chem. Res.* **2013**, *46*, 1616−1626.
(31) Meng, F.; Jin, S. The Solution Growth of Copper Nanowires and Nanotubes is Driven by Screw Dislocations. *Nano Lett.* **2012**, *12*, 234−239.
(32) Wu, H.; Meng, F.; Li, L.; Jin, S.; Zheng, G. Dislocation-Driven CdS and CdSe Nanowire Growth. *ACS Nano* **2012**, *6*, 4461−4468.
(33) Ramiro-Manzano, F.; García-Aboal, R.; Fenollosa, R.; Biasi, S.; Rodriguez, I.; Atienzar, P.; Meseguer, F. Optical properties organic/inorganic perovskite microcrystals through the characterization of Fabry-Pérot resonances, to be submitted, 2018.
(34) Heo, J. H.; Song, D. H.; Im, S. H. Planar CH3NH3PbBr3 Hybrid Solar Cells with 10.4% Power Conversion Efficiency, Fabricated by Controlled Crystallization in the Spin-Coating Process. *Adv. Mater.* **2014**, *26*, 8179−8183.


DOI: 10.1021/acsomega.8b00447
*ACS Omega* 2018, 3, 5229−5236